Geothermal input significantly influences riverine and oceanic boron budgets

Jun Xiao[1], Zhiqi Zhao[2], Julien Bouchez[3], Xiaolin Ma[1], Philip A. E. Pogge von Strandmann[4], Daisuke Araoka[5], Toshihiro Yoshimura[6], H. M. Zakir Hossain[7], Hodaka Kawahata[8], and Zhang-dong Jin[1,9*]

[1]*SKLLQG, Institute of Earth Environment, Chinese Academy of Sciences, Xi'an, 710061, China;*

[2]*School of Earth Science and Resources, Chang'an University, Xi'an 710054, China;*

[3]*Université de Paris, Institut de physique du Globe de Paris, CNRS, F-75005 Paris, France;*

[4]*Institute of Geosciences, Johannes Gutenberg-Universitat Mainz, 55128 Mainz, Germany;*

[5]*Geological Survey of Japan, National Institute of Advanced Industrial Science and Technology (AIST), Japan;*

[6]*Japan Agency for Marine-Earth Science and Technology (JAMSTEC), Japan;*

[7]*Department of Petroleum and Mining Engineering, Jashore University of Science and Technology, Bangladesh;*

[8]*Atmosphere and Ocean Research Institute, The University of Tokyo, Japan;*

[9]*Institute of Global Environmental Change, Xi'an Jiaotong University, Xi'an710049, China*

[*]Corresponding author: zdjin523@hotmail.com

Abstract: The evolution of boron isotope compositions of seawater ($\delta^{11}B_{sw}$) over the Cenozoic has important implications for reconstructions of atmospheric CO_2 and is tightly linked to boron input from the Himalaya-Tibetan Plateau. However, controls on evolution in $\delta^{11}B_{sw}$ remain elusive. We report geochemical measurements of the Yarlung Tsangpo River draining the Tibetan Plateau and observe exceptionally high riverine boron concentrations and extremely low $\delta^{11}B$ values. Calculation indicates that >50% of riverine boron is sourced from geothermal waters. Combined with global datasets, we show that global riverine boron input to the ocean is largely influenced by geothermal input. Mass-balance calculations indicate that an averaged 1.5-fold decrease in global geothermal inputs is sufficient to introduce 3‰ increase in Cenozoic $\delta^{11}B_{sw}$. Therefore, geothermal waters significantly affect global riverine and thus oceanic boron budgets. The increased $\delta^{11}B_{sw}$ since Cenozoic is resulted partly from declining global geothermal activity.

Key Words: boron isotope, chemical weathering, geothermal water input, boron budgets, Yarlung Tsangpo River

1. Introduction

The uplift of the Himalayas-Tibetan Plateau is thought to have played a critical role in the global evolution of continental denudation and weathering, global geochemical cycles, atmospheric CO_2, and climate shift over the Cenozoic (Raymo and Ruddiman, 1992; Li and Elderfield, 2013; Yao et al., 2013). One of the important proxies used to reconstruct past atmospheric CO_2 levels over such long geological timescales is the isotopic composition of boron ($\delta^{11}B$) in marine carbonates, that responds to both the oceanic pH (controlled by dissolved CO_2 concentration and alkalinity) and $\delta^{11}B$ of seawater (Hemming and Hanson, 1992; Pearson and Palmer, 2000; Clarkson et al., 2015; Greenop et al., 2017). Due to the lack of reliable independent records (Greenop et al., 2017), constraints on the B isotope ratio of the seawater ($\delta^{11}B_{sw}$) largely depended on models of global geochemical cycles that heavily rely on assumption the flux and $\delta^{11}B$ of river water (Lemarchand et al., 2000). However, the factors that controlling flux and $\delta^{11}B$ of river water are subjected to large debates.

This work investigates the boron isotopic systematics in the Yarlung Tsangpo River, the largest river system on the Tibetan Plateau. The uplift of the Himalayas-Tibetan Plateau is thought to have played a critical role in the global evolution of ocean chemistry (e.g., Sr, Os, and Li isotopic composition of seawater; Edmond, 1992; Galy et al., 1999; Klemm et al., 2005; Misra and Froelich, 2012) due to the large weathering flux associated with uplift and the unique geological/geochemical of the uplifting terrains. Rivers draining the Himalaya-Tibetan Plateau contribute >17% of the global B input into the oceans (Lemarchand et al., 2000, 2002). We also expect very unique boron isotopic composition of the Tibetan River since the tectonically active Himalaya-Tibetan Plateau is characterized by widespread hydrothermalism, which significantly impacts the geochemical compositions of rivers in the area (Evans et al., 2001, 2004; Hren et al., 2007; Lü et al., 2014; Zhang et al., 2015, 2021, 2022). Given that geothermal waters usually have high B concentrations and low $\delta^{11}B$ values (Palmer et al., 1990; Evans et al., 2004; Millot et al., 2012; Louvat et al., 2014), even slight changes in geothermal activity in the Himalaya-Tibetan Plateau may substantially impacts the global oceanic B budget. However, the contribution of continental hydrothermalism to the global riverine B remains poorly constrained.

Here, we quantify the contribution of dissolved B sourced from geothermal waters to Himalayan rivers using samples systematically collected from the Yarlung Tsangpo River. Then, we compile a global dataset of both riverine and geothermal waters to constrain weathering and geothermal endmember contribution to the flux and $\delta^{11}B$ of global rivers. Finally, we address possible contributions of geothermal waters to long-term seawater B budget and $\delta^{11}B_{sw}$ evolution over the Cenozoic using a sensitive test.

2. Study area

As one of the major tributaries of the Brahmaputra, the Yarlung Tsangpo River flows over a distance of 2,093 km along the depression of the Indus-Tsangpo Suture (Fig. 1), draining an area of 23.8×10^4 km^2 in which numerous geothermal springs have been reported (Lü et al., 2014; Liu et al., 2020). This river basin, affected by the Indian summer monsoon, exhibits a clear longitudinal climate gradient with a mean annual precipitation < 300 mm in the western part, 300-600 mm in the middle part, and > 2000 mm in the eastern part (Fig. 2). Air temperature also increases from west to east, with a basin average mean annual temperature of 5.9 °C (Fig. 2). The Yarlung Tsangpo River is mainly fed by monsoonal rainfall from June to September, as well as by glacier melting and geothermal waters. The geology of the southern part of the basin is dominated by the Tethyan Sedimentary Series, the northwestern part is underlain by the Tertiary volcanic, and the northeastern part drains Cretaceous-Tertiary granitic plutons and the Lhasa block (Singh et al., 2006). There are several N-S-striking rifts in the Yarlung Tsangpo drainage, such as the Dingri-Nima, Dingjie-Xietongmen-Shenzha, Yadong-Dangxiong-Gulu, and Gudui-Sangri rifts (Fig. 1). Geothermal water often occurs in these rift zones, some of which can discharge into the Yarlung Tsangpo River directly (Zhang et al., 2022). For example, geothermal water in the Semi and Dagejia geothermal fields flow directly into the stem and tributary of the Yarlung-Tsangpo River, respectively.

3. Materials and Methods

3.1. Sampling

Fifty-one river water samples were collected from the Yarlung Tsangpo River in June (dry season) and September (wet season), 2017 (Fig. 1). Seventeen geothermal waters and three rainwater samples were also collected within the basin in July. The river water samples of B1 (13 Jan. 2011), B2 (12 Jan. 2011) and B3 (14 Jan. 2011; 14 Feb. 2012) in the lower Brahmaputra above its convergence with the Ganges were collected (Manaka et al., 2017). All water samples were filtered *in situ* using 0.45-μm porosity nylon membrane Millipore filters. The temperature, pH, and electrical conductivity (EC) were determined *in situ* using a portable Orion EC/pH meter. For cations, trace elements, and boron isotopes analysis, 500 mL of filtered water were stored in HDPE bottles and acidified to pH < 2 by double-distilled GR HNO_3. For anion measurements, 500 mL of filtered water was stored in HDPE bottles. All water samples were stored at 4 °C until analysis. The cations (Ca^{2+}, Na^+, Mg^{2+}, K^+, and SiO_2) were detected by ICP-OES (Varian Vista-MPX) and anions (Cl^-, NO_3^-, and SO_4^{2-}) were detected by ion chromatography (Dionex ICS-90). Two suspended particulate matters (SPM) of sample M29 and M1 and 5 bank sediment samples at the sampling sites of M11, M17, M19, T10, and T18 were also collected for comparisons (Fig. 1). The SPM collected on the filters was removed in the clean laboratory using boron free Millipore Milli-Q water. Solutions containing the SPM were evaporated gently at 55 °C. Then, SPM and bank sediments samples were crushed in agate mortar after drying. SPM and bank sediment samples were digested by alkali fusion (Chetelat et al., 2009).

3.2. Boron concentration and δ^{11}B analyses

B concentrations and δ^{11}B were analyzed using a PE 300D ICP-MS and a Thermo Neptune Plus MC-ICP-MS at the Institute of Earth Environment, Chinese Academy of Sciences (IEECAS), respectively. Before δ^{11}B measurements, B was purified from the samples matrix by ion chromatography using the B-specific anion resin of Amberlite IRA 743. Before loading samples onto the column, the solution pH was adjusted to 6-7 and the resin was conditioned with 0.3 M $NH_3 \cdot H_2O$, before being rinsed using Milli-Q water. Finally, 500 ng B was eluted by 5 mL 2% HNO_3. For a solution with a B concentration of 100 ng/g, the ^{11}B ion intensity was measured at ~1.0 V, while the blank value of 2% HNO_3 was ~4 mV. A washout time of 240 s was used to reduce the B signal to <1% of the signal achieved for standards and samples at 100 ng/g of B. Boron isotope composition was measured using the standard-sample bracketing (SSB) method. The reference materials NIST SRM 951, ERM AE 121 and ERM AE 122 were included in measurement sequences to check for measurement accuracy and reproducibility. The measured values are presented in delta notation relative to NIST SRM 951:

$$\delta^{11}B = [(^{11}B/^{10}B)_{sample}/(^{11}B/^{10}B)_{standard} - 1] \times 1000$$

The $\delta^{11}B$ of repeated NIST SRM 951 was 0.01‰ (2 s.d.=0.20‰, n=40). The $\delta^{11}B$ of repeated ERM AE 121 was +20.1‰ (1 s.d.=0.37‰, n=18), and ERM AE 122 was +39.5 ± 0.6‰ (2 s.d., n=40), which are consistent with their certified values of +19.9‰ and +39.7‰, respectively (Vogl and Rosner, 2012).

4. Results

The $[B]_{rw}$ of the investigated river water of Yarlung Tsangpo River straddles four orders of magnitude ranging from 0.16 to 371 μmol/L (median 34.7 μmol/L; average 72.5 μmol/L), which is much higher than the worldwide riverine average of 0.9 μmol/L (Lemarchand et al., 2002). The $\delta^{11}B_{rw}$ values in the Yarlung Tsangpo River range from -14.4 to +0.9‰ (averaging -9.2‰), which is substantially lower than other globally large rivers (averaging +10‰) (Fig. 3; Rose et al., 2000; Lemarchand et al., 2002; Chetelat and Gaillardet, 2005; Lemarchand and Gaillardet, 2006; Chetelat et al., 2009; Liu et al., 2012; Louvat et al., 2011, 2014; Ercolani et al., 2019). Our dataset reports the highest $[B]_{rw}$ (tributary sample T10 in dry season) and lowest $\delta^{11}B_{rw}$ values (mainstream M11 in wet season) of river water measured to date (Fig. 1). The $[B]_{rw}$ decreases while $\delta^{11}B_{rw}$ increases downstream, with overall lower values during the wet season (Fig. 4). The [B] and $\delta^{11}B$ of geothermal water within the Yarlung Tsangpo River Basin varies from 15.6 to 8580 μmol/L and from -16.0 to -0.1‰, with median of 2800 μmol/L and -8.6‰, respectively (Table S1). These values are in agreement with previous measurements (Lü et al., 2014; Zhang et al., 2015; Fig. 3). Three rainwater samples show [B] of 0.13 μmol/L, 0.58 μmol/L, and 0.62 μmol/L, much lower than most of the Yarlung Tsangpo River. The $\delta^{11}B$ values of three rainwater samples are +0.2‰, -2.7‰ and -3.4‰, higher than that of the Yarlung Tsangpo River (Fig. 4b).

Two SPM samples show [B] and $\delta^{11}B$ of 123 and 40.1 μg/g, and -5.3‰ and -5.2‰, respectively. The [B] and $\delta^{11}B$ of five sediments samples varies between 15.8 μg/g and 25.0 μg/g and between -10.2‰ and -6.3‰, with an average value of 21.3 μg/g and -7.4‰, respectively (Table S1).

5. Discussion

5.1. B source and geothermal contribution

Owing to limited human activities within the basin, anthropogenic input to riverine B is minor. Based on a B/Cl molar ratio in local precipitation of 0.02 (Rose et al., 2000), the atmospheric input is calculated to be 4.9 ($^{+8.7}/_{-3.5}$)% (superscript and subscript quantify uncertainty and represent the 25th and 75th percentiles of the calculated probability distribution, respectively) with lower values in upstream. This spatial variability of atmospheric contribution is in line with the precipitation gradient in the basin (Fig. 2). Furthermore, based on B/SO_4 and B/Ca molar ratios (Chetelat and Gaillardet, 2005; Lemarchand and Gaillardet, 2006), the combined contribution of evaporite dissolution and carbonate weathering to riverine B is estimated at 1.2 ($^{+2.6}/_{-0.9}$)%. Previous studies on $\delta^{11}B_{rw}$ in large rivers have shown that silicate weathering at the Earth's surface typically results in higher $\delta^{11}B_{rw}$ values than those of river SPM and sediments, due to the preferential release of ^{11}B to waters and retention of ^{10}B in secondary phases such as clays (Gaillardet and Lemarchand, 2018). This is in stark contrast with our results, as $\delta^{11}B_{rw}$ values in the Yarlung Tsangpo River are generally lower than $\delta^{11}B$ values of SPM and bank sediments (Table S1). This observation indicates that surficial silicate weathering, as typified in soils, is not the dominant source of dissolved B in the Yarlung Tsangpo River.

Geothermal waters sampled in the Yarlung Tsangpo Basin are characterized by high B concentrations ($[B]_{gw}$, 2780 ($^{+1771}/_{-2409}$) μmol/L) but low $\delta^{11}B$ ($\delta^{11}B_{gw}$, -8.8 ($^{+4.1}/_{-1.7}$)‰ (Fig. 3). The geothermal waters are enriched with arsenic (As) and the elevated riverine As concentrations ($[As]_{rw}$) in the Yarlung Tsangpo River have been shown to be related to geothermal water inputs (Li et al., 2013; Zhang et al., 2021). The strong positive correlation between $[B]/[Cl]_{rw}$ and $[As]/[Cl]_{rw}$ supports that the high $[B]_{rw}$ and low $\delta^{11}B_{rw}$ observed here across the Yarlung Tsangpo Basin is also due to geothermal water inputs (Fig. 4a). Based on B/Cl molar ratio measured in geothermal water samples near the river sampling sites, the calculated contribution of geothermal waters to river dissolved B is 72.0 ($^{+79.5}/_{-59.9}$)%.

The spatial pattern of $[B]_{rw}$ and $\delta^{11}B_{rw}$ within the Yarlung Tsangpo Basin is also consistent with a significant influence of geothermal waters on river chemistry there (Fig. 2b). Snow-melt waters and rainfall in the Yarlung Tsangpo Basin have relatively low B concentrations and high $\delta^{11}B$ values, compared to those of the geothermal waters (Fig. 4b). As a consequence, eastward trend towards a wetter climate (more snow-melt and rainfall) lead to a downstream decrease of $[B]_{rw}$ through dilution, together with an increase in $\delta^{11}B_{rw}$, thus determining the observed spatial gradients in $[B]_{rw}$ and $\delta^{11}B_{rw}$ in the basin (Fig. 2). This inference is also supported by the negative relationship between instantaneous water discharge (Q_w), which increases with rainfall inputs, and $[B]_{rw}$ (Fig. 4c), as well as by the positive relationship between Q_w and $\delta^{11}B_{rw}$ during both seasons (Fig. 4d). In addition, $\delta^{11}B_{rw}$ values in the wet season and dry season have similar range and variation trend in Fig. 4b, where the B/Cl can minimize the effect of dilution. Therefore, discharge can dilute $[B]_{rw}$ while it exerts minor influence on $\delta^{11}B_{rw}$. The higher $\delta^{11}B$ values in the dry season than the wet season (Fig. 4f) was related with B isotope fractionation under different discharge. The very fast flow at high discharge in wet season would lead to the shorter water-rock interactions than in dry season. Therefore, less ^{10}B is incorporated into the secondary minerals in the river as SPM or bed sediments in wet season, resulting in lower riverine $\delta^{11}B$. Despite an increasing downstream trend of $\delta^{11}B_{rw}$ in the Yarlung Tsangpo River, the relatively invariant $\delta^{11}B_{rw}$ values observed at the outlet of the Brahmaputra (samples B1, B2, and B3 in Fig. 1 and Table S1, $\delta^{11}B_{rw}$=-6.5‰) are still much lower than those of the other large rivers (Fig. 3).

Importantly, the $\delta^{11}B_{rw}$ values of other rivers originating from the Tibetan Plateau, such as the Salween (-3.11‰), the Mekong (+2.31‰), the Yangtze (+4.10‰), and the Yellow River (+5.15‰), are all potentially impacted by similar geothermal inputs because they drain the same area, considering their lower than the world average $\delta^{11}B_{rw}$ value (Lemarchand et al., 2002). At the global scale, geothermal waters with relatively high $[B]_{gw}$ and low $\delta^{11}B_{gw}$ have also been reported in tectonically active regions including volcanic islands, such as Guadeloupe, Réunion, Iceland, New

Zealand, and Taiwan (Aggarwal et al., 2000; Louvat et al., 2011, 2014; Liu et al., 2012; Millot et al., 2012; Fig. 3). Collectively, these observations lend support to our interpretation for the low $\delta^{11}B_{rw}$ values in the Yarlung Tsanpo River, and warrant a quantitative examination of the potential impact of continental hydrothermalism on global riverine and oceanic $\delta^{11}B$.

5.2. B budget of geothermal water input to the ocean

We develop a mass balance model to explore the potential effects of historical global changes in geothermal inputs on the observed ~3‰ increase in seawater $\delta^{11}B_{sw}$ throughout the Cenozoic era to the present day (Greenop et al., 2017; Gaillardet and Lemarchand, 2018; Sosdian et al., 2018).

Given that geothermal water inflows to the ocean through river systems, our study initially test the contribution of geothermal water B to the global riverine B content and its impact on the global river $\delta^{11}B$ ($\delta^{11}B_{riv}$). Subsequently, we evaluated the cumulative influence of geothermal water B on seawater $\delta^{11}B$ ($\delta^{11}B_{sw}$). Our underlying assumption was that global riverine B is sourced from two principal origins: continental weathering and geothermal inputs, denoted as $\delta^{11}B_w$ and $\delta^{11}B_{gw}$ respectively. The $\delta^{11}B_{riv}$ can be expressed as follows:

$$\delta^{11}B_{riv} \times (F_{gw} + F_w) = \delta^{11}B_{gw} \times F_{gw} + \delta^{11}B_w \times F_w \qquad (1)$$

where F_{gw} and F_w represent the relative mass contributions of geothermal waters and weathering materials to the annual global riverine B flux. According to the dataset provided by Lemarchand et al. (2002), the contemporary global riverine B influx into the ocean ($F_{gw} + F_w$) is estimated to be 0.38 TgB/yr, exhibiting a $\delta^{11}B_{riv}$ value of +10‰. Moreover, a mean $\delta^{11}B$ of geothermal water B ($\delta^{11}B_{gw}$) value of -6.8‰ was derived from a comprehensive compilation of data originating from tectonically active regions (132 data entries) and used as $\delta^{11}B_{gw}$ baseline value (Palmer and Sturchio, 1990; Kasemann, 2004; Millot et al., 2012; Louva et al., 2014; Lü et al., 2014; Zhang et al., 2015; Sosdian et al., 2018). Because of the limited data availability of geothermal water and weathering fluxes, the direct estimation of global geothermal water inputs relative to weathering-derived B in global rivers proves challenging. Nevertheless, by employing Equation (1) in conjunction with riverine B influx into the ocean (0.38 TgB/yr) and the average $\delta^{11}B_{riv}$ value (+10‰), as long as one of the four parameters of F_{gw}, F_w, $\delta^{11}B_{gw}$ and $\delta^{11}B_w$ is given, the remaining three parameters can be calculated. Subsequently, the sensitivity of seawater $\delta^{11}B_{sw}$ to geothermal water inputs can be examined.

In this study, we adopted two extreme scenarios to estimate these fluxes. The Brahmaputra Basin was identified as a source of 0.02 TgB/yr (F_{gw}) of geothermal B, constituting approximately 5% of riverine B (Lemarchand et al., 2002). In the absence of information regarding geothermal water B contributions from other regions, we adopted the boron inputs from the Brahmaputra Basin as the lower limit estimate for the contribution of geothermal water B to riverine B. Consequently, we can derive the weathering flux (F_w,) to be 0.36 TgB/yr, accounting for approximately 95% of riverine B, accompanied by a $\delta^{11}B_w$ value of +10.6‰, representing the upper limit for F_w and lowest limit for $\delta^{11}B_w$.

Conversely, in another extreme scenario, the highest reported weathering $\delta^{11}B$ value (+43‰) by Lemarchand et al. (2002) was adopted as an estimate for highest limit for $\delta^{11}B_w$. This led to estimates of F_{gw} and F_w amounting to 0.25 TgB/yr and 0.13 TgB/yr, respectively, as calculated through Equation (1). This scenario indicates that geothermal inputs account for approximately 66% of global riverine B inflows into the ocean. Therefore, we employed 5% and 66% as the respective lower and upper bounds for global geothermal water B to riverine B. The potential impact of geothermal inputs on seawater $\delta^{11}B_{sw}$ via global rivers was calculated using the following Equation (2):

$$\delta^{11}B_{sw\text{-}0} \times M + \delta^{11}B_{gw} \times \Delta F_{gw} \times T = \delta^{11}B_{sw} \times (M + \Delta F_{gw} \times T) \qquad (2)$$

here, $\delta^{11}B_{sw\text{-}0}$ and $\delta^{11}B_{sw}$ represent the initial and geothermal water enhanced seawater $\delta^{11}B$ values, respectively, T represents the residence time of seawater B (1.4×10^7 yr), and M denotes the seawater B inventory (6.2×10^5 TgB; Lemarchand et al., 2000). ΔF_{gw} denotes changes in geothermal inputs to the ocean. We also define the $\Delta^{11}B_{sw}$ as the alterations in seawater $\delta^{11}B_{sw}$ due to shifts in geothermal inputs to the ocean, expressed as $\Delta^{11}B_{sw} = \delta^{11}B_{sw} - \delta^{11}B_{sw\text{-}0}$. Assuming a constant seawater B inventory (M) during the past, that is, $(M + \Delta F_{gw} \times T)$ in the Equation (2) can be replaced by M. And then, we bring $\Delta^{11}B_{sw}$ into the Equation (2), thereby the mass balance model can be simplified to the following Equation (3):

$$\Delta^{11}B_{sw} = \Delta F_{gw} \times \delta^{11}B_{gw} \times T / M \quad (3)$$

For the lower bound estimate of geothermal contribution to seawater $\delta^{11}B$, a tenfold increase in flux (from 0.02 TgB/yr (5%) to 0.21 TgB/yr (37%); indicated by the green arrow in Fig. 5a) of geothermal water input to global runoff proves sufficient to account for the observed 3‰ decline in seawater $\delta^{11}B$ ($\Delta^{11}B$) from the present to the early Cenozoic. At the upper limits of current global geothermal inputs to riverine B, even a modest 0.8-fold increase in flux (from 0.25 TgB/yr (66%) to 0.45 TgB/yr (77%); indicated by the blue arrow in Fig. 5a) of geothermal water input into global rivers provides an explanation for the 3‰ decrease in $\Delta^{11}B$ from the present to the early Cenozoic. On average, a 1.5-fold enhancement in geothermal water fluxes (from 0.13 to 0.33 TgB/yr) into global runoff sufficiently explains the 3‰ decrease in $\Delta^{11}B$ from the present to the early Cenozoic (Fig. 5a), assuming comparable B isotopic compositions for weathering products and geothermal waters during the Cenozoic. Alternatively, the dynamic evolution of seawater $\delta^{11}B_{sw}$ throughout the Cenozoic may have been jointly influenced by both weathering products and geothermal water inflow into the ocean.

5.3. The role of geothermal input in Cenozoic seawater $\delta^{11}B$ evolution

The collision between the Indian plate and the Eurasian plate in the early Cenozoic was associated with significant magmatism (Hu et al., 2016; Guo et al., 2021), which has potentially led to enhanced geothermal water inputs into the rivers and oceans. Thus, the geothermal activity related to the Indian-Eurasian collision over the Cenozoic may have affected the delivery of elements associated with geothermal inputs into rivers. We propose that the relatively low $\delta^{11}B_{sw}$ in the early Cenozoic is at least partially a result of such input of enhanced geothermal water with low $\delta^{11}B_{gw}$, besides potential changes in surficial silicate weathering. Enhanced geothermal water inputs in the early Cenozoic are further supported by strong collision-related magmatism in Tibet in the same period, as reflected by the melting degree based on geothermal data (Fig. 5b; Guo et al., 2021). Indeed, the melting degree showed substantially decreased magmatic activity since the last 50 Ma (Fig. 5b; Guo et al., 2021). This would result in decreased geothermal output to rivers and the oceans. As a consequence, the secular evolution of oceanic $\delta^{11}B$ since the Cenozoic should take into account the potential role of variations in geothermal waters.

6. Conclusions

Based on the analysis of major ions, boron concentration and isotopic compositions, we observe that the boron concentrations are exceptionally high while $\delta^{11}B$ values are extremely low in the Yarlung Tsangpo River. Due to a wetter climate and the dilution downstream, the $[B]_{rw}$ shows deceasing trend while $\delta^{11}B_{rw}$ shows an increasing trend from upstream to downstream. The lower $\delta^{11}B_{rw}$ values of river water than SPM and bank sediments, and the strong positive correlation between riverine B/Cl and As/Cl support that geothermal water input influences the boron geochemistry in the Yarlung Tsangpo River (Fig. 4a). Further, the contribution calculation indicates that more than half of boron in the Yarlung Tsangpo River is sourced from geothermal waters. Based on a sensitive test of mass-balance calculations, we observe that geothermal input significantly affects global riverine and oceanic boron budgets, and an averaged 1.5-fold decrease in global geothermal inputs is sufficient to introduce 3‰ increase in Cenozoic $\delta^{11}B_{sw}$. Compared with collision-related magmatism in the Tibet, we propose that the increased $\delta^{11}B_{sw}$ since Cenozoic is resulted partly from declining global geothermal activity.

Acknowledgments

We thank J. Guo, L. Zhang, R. Ye, S. Gao, J. Meng, T. Liu, L. Cui, X. Zhang, G. Jia, and Y. Yang for their help during the sample collection. This work was financially supported by NSFC (41991322, 41661144042), and the Second Tibetan Plateau Scientific Expedition and Research

(STEP 2019QZKK0707).

Author Contributions:

Jun Xiao: Data curation, Formal analysis, Methodology, Resources, Writing-original draft, Writing-review & editing. **Zhiqi Zhao:** Conceptualization, Data curation, Investigation, Methodology, Resources, Project administration, Funding acquisition, Writing-review & editing. **Julien Bouchez:** Data curation, Methodology, Writing-review & editing. **Xiaolin Ma:** Conceptualization, Data curation, Methodology, Writing-review & editing. **Philip A. E. Pogge von Strandmann:** Data curation, Methodology, Writing-review & editing. **Daisuke Araoka:** Methodology, Resources, Writing-review & editing. **Toshihiro Yoshimura:** Methodology, Resources, Writing-review & editing. **H. M. Zakir Hossain:** Methodology, Resources, Writing-review & editing. **Hodaka Kawahata:** Methodology, Resources, Writing-review & editing. **Zhangdong Jin:** Conceptualization, Funding acquisition, Methodology, Resources, Project administration, Supervision, Validation, Writing-original draft, Writing-review & editing.

Declaration of competing interest

The authors declare that they have no known competing financial interests or personal relationships that could have appeared to influence the work reported in this paper.

References

Aggarwal, J. K., Palmer, M. R., Bullen, T. D., Arnórsson, S., & Ragnarsdóttir, K. V. (2000). The boron isotope systematics of Icelandic geothermal waters: 1. Meteoric water charged systems. *Geochimica et Cosmochimica Acta, 64*, 579-585. https://doi.org/10.1016/S0016-7037(99)00300-2

Chetelat, B., & Gaillardet, J. (2005). Boron isotopes in the Seine River, France: a probe of anthropogenic contamination. *Environmental Science & Technology, 39*, 2486-2493. https://doi: 10.1021/es048387j

Chetelat, B., Liu, C. Q., Gaillardet, J., Wang, Q. L., Zhao, Z. Q., Liang, C. S., et al. (2009). Boron isotopes geochemistry of the Changjiang basin rivers. *Geochimica et Cosmochimica Acta, 73*, 6084-6097. https://doi.org/10.1016/j.gca.2009.07.026

Clarkson, M. O., Kasemann, S. A., Wood, R. A., Lenton, T. M., Daines, S. J., Richoz, S., et al. (2015). Ocean acidification and the Permo-Triassic mass extinction. *Science, 348*, 229-232. https://doi: 10.1126/science.aaa0193

Edmond, J. M. (1992). Himalayan tectonics, weathering processes, and the strontium isotope record in marine limestones. *Science, 258*, 1594-1597. https://www.jstor.org/stable/2882056

Ercolani, C., Lemarchand, D., & Dosseto, A. (2019). Insights on catchment-wide weathering regimes from boron isotopes in riverine material. *Geochimica et Cosmochimica Acta, 261*, 35-55. https://doi.org/10.1016/j.gca.2019.07.002

Evans, M. J., Derry, L. A., Anderson, S. P., & France-Lanord, C. (2001). Hydrothermal source of radiogenic Sr to Himalayan rivers. *Geology, 29*, 803-806. https://doi.org/10.1130/0091-7613(2001)029<0803:HSORST>2.0.CO;2

Evans, M. J., Derry, L. A., & France-Lanord, C. (2004). Geothermal fluxes of alkalinity in the Narayani river system of central Nepal. *Geochemistry, Geophysics, Geosystems, 5*, Q08011, doi:10.1029/2004GC000719. https://doi.org/10.1029/2004GC000719

Gaillardet, J., & Lemarchand, D. (2018). Boron in the Weathering Environment. In: Marschall, H., Foster, G. (eds) Boron Isotopes. Advances in Isotope Geochemistry. Springer, Cham. https://doi.org/10.1007/978-3-319-64666-4_7

Galy, A., France-Lanord, C., & Derry, L. A. (1999). The strontium isotopic budget of Himalayan rivers in Nepal and Bangladesh. *Geochimica et Cosmochimica Acta, 63*, 1905-1925. https://doi.org/10.1016/S0016-7037(99)00081-2

Greenop, R., Foster, G. L., Sosdian, S. M., Hain, M. P., Oliver, K. I. C., Goodwin, P., et al. (2017). A record of Neogene seawater δ^{11}B reconstructed from paired δ^{11}B analyses on benthic and planktic foraminifera. *Climate of the Past, 13*,149-170. https://doi.org/10.5194/cp-13-149-2017

Guo, Z., Wilson, M., Dingwell, D. B., & Liu, J. (2021). India-Asia collision as a driver of atmospheric CO_2 in the Cenozoic. *Nature Communications, 12*, 3891. https://doi.org/10.1038/s41467-021-23772-y

Hemming, N. G., & Hanson, G. N. (1992). Boron isotopic composition and concentration in modern marine carbonates. *Geochimica et Cosmochimica Acta, 56*, 537-543. https://doi.org/10.1016/0016-7037(92)90151-8

Hren, M. T., Chamberlain, C. P., Hilley, G. E., Blisniuk, P. M., & Bookhagen, B. (2007). Major ion chemistry of the Yarlung-Brahmaputra river: Chemical weathering, erosion, and CO_2 consumption in the southern Qinghai-Tibet plateau and eastern syntaxis of the Himalaya. *Geochimica et Cosmochimica Acta, 71*, 2907-2935. https://doi.org/10.1016/j.gca.2007.03.021

Hu, X. M., Garzanti, E., Wang, J. G., Huang, W. T., An, W., & Webb, A. (2016). The timing of India-Asia collision onset-Facts, theories, controversies. *Earth-Science Reviews, 160*, 264-299. https://doi.org/10.1016/j.earscirev.2016.07.014

Kasemann, S. A., Meixner, A., Erzinger, J., Viramonte, J. G., Alonso, R. N., & Franz, G. (2004). Boron isotope composition of geothermal fluids and borate minerals from salar deposits (central Andes/NW Argentina). *Journal of South American Earth Sciences, 16*, 685-697. https://doi.org/10.1016/j.jsames.2003.12.004

Klemm, V., Levasseur, S., Frank, M., Hein, J. R., & Halliday, A. N. (2005). Osmium isotope stratigraphy of a marine ferromanganese crust. *Earth and Planetary Science Letters, 238*, 42-48. https://doi.org/10.1016/j.epsl.2005.07.016

Lemarchand, D., Gaillardet, J., Lewin, E., & Allegre, C. J. (2000). The influence of rivers on marine boron isotopes and implications for reconstructing past ocean pH. *Nature, 408*, 951-954. https://doi.org/10.1038/35050058

Lemarchand, D., Gaillardet, J., Lewin, E., & Allegre, C. J. (2002). Boron isotope systematics in large rivers: implications for the marine boron budget and paleo-pH reconstruction over the Cenozoic. *Chemical Geology, 190*, 123-140. https://doi.org/10.1016/S0009-2541(02)00114-6

Lemarchand, D., & Gaillardet J. (2006). Transient features of the erosion of shales in the Mackenzie basin (Canada), evidences from boron isotopes. *Earth and Planetary Science Letters, 245*, 174-189. https://doi.org/10.1016/j.epsl.2006.01.056

Li, G. J., & Elderfield, H. (2013). Evolution of carbon cycle over the past 100 million years. *Geochimica et Cosmochimica Acta, 103*, 11-25. https://doi.org/10.1016/j.gca.2012.10.014

Li, S. H., Wang, M. G., Yang, Q., Wang, H., Zhu, J. M., Zheng, B. S., et al. (2013). Enrichment of arsenic in surface water, stream sediments and soils in Tibet. *Journal of Geochemical Exploration,135*, 104-116. http://dx.doi.org/10.1016/j.gexplo.2012.08.020

Liu, M. L., Guo, Q. H., Luo, L., & He, T. (2020). Environmental impacts of geothermal waters with extremely high boron concentrations: Insight from a case study in Tibet, China. *Journal of Volcanology and Geothermal Research, 397*, 106887. https://doi.org/10.1016/j.jvolgeores.2020.106887

Liu, Y. C., You, C. F., Huang, K. F., Wang, R. M., Chung, C. H., & Liu, H. C. (2012). Boron sources and transport mechanisms in river waters collected from southwestern Taiwan: Isotopic evidence. *Journal of Asian Earth Sciences, 58*, 16-23. https://doi.org/10.1016/j.jseaes.2012.07.008

Louvat, P., Gaillardet, J., Paris, G., & Dessert, C. (2011). Boron isotope ratios of surface waters in Guadeloupe, Lesser Antilles. *Applied Geochemistry, 26*, S76-S79. https://doi.org/10.1016/j.apgeochem.2011.03.035

Louvat, P., Gayer, E., & Gaillardet, J. (2014). Boron behavior in the rivers of Réunion island, inferred from boron isotope ratios and concentrations of major and trace elements. *Procedia Earth and Planetary Science, 10*, 231-237. https://doi.org/10.1016/j.proeps.2014.08.029

Lü, Y. Y., Zheng, M. P., Zhao, P., & Xu, R. H. (2014). Geochemical processes and origin of boron isotopes in geothermal water in the Yunnan-Tibet geothermal zone. *Science China-Earth Sciences,* 57, 2934-2944. https://doi.org/10.1007/s11430-014-4940-2

Manaka, T., Araoka, D., Yoshimura, T., Hossain, H. M. Z., Nishio, Y., Suzuki, A., et al. (2017). Downstream and seasonal changes of lithium isotope ratios in the Ganges-Brahmaputra river system. *Geochemistry, Geophysics, Geosystems, 18*, 3003-3015. https://doi.org/10.1002/2016GC006738

Millot, R., Hegan, A., & Négrel, P. (2012). Geothermal waters from the Taupo Volcanic Zone, New Zealand: Li, B and Sr isotopes characterization. *Applied Geochemistry, 27*, 677-688. https://doi.org/10.1016/j.apgeochem.2011.12.015

Misra, S., & Froelich, P.N. (2012). Lithium isotope history of Cenozoic seawater: Changes in silicate weathering and reverse weathering. *Science*, *335*, 818-823. https://doi: 10.1126/science.1214697

Palmer, M. R., & Sturchio, N. C. (1990). The boron isotope systematics of the Yellowstone National Park (Wyoming) hydrothermal system: A reconnaissance. *Geochimica et Cosmochimica Acta, 54*, 2811-2815. https://doi.org/10.1016/0016-7037(90)90015-D

Pearson, P. N., & Palmer, M. R. (2000). Atmospheric carbon dioxide concentrations over the past 60 million years. *Nature, 406*, 695-699. https://doi.org/10.1038/35021000

Raymo, M.E., & Ruddiman, W.F. (1992). Tectonic forcing of late Cenozoic climate. *Nature, 359*, 117-122. https://doi.org/10.1038/359117a0

Rose, E.F., Chaussidon, M., & France-lanord, C. (2000). Fractionation of boron isotopes during erosion processes: The example of Himalayan rivers. *Geochimica et Cosmochimica Acta, 64*, 397-408. https://doi.org/10.1016/S0016-7037(99)00117-9

Singh, S. K., Kumar, A., & France-Lanord, C. (2006). Sr and $^{87}Sr/^{86}Sr$ in waters and sediments of the Brahmaputra river system: Silicate weathering, CO_2 consumption and Sr flux. *Chemical Geology, 234*, 308-320. https://doi.org/10.1016/j.chemgeo.2006.05.009

Sosdian, S. M., Greenop, R., Hain, M. P., Foster, G. L., Pearson, P. N., & Lear, C. H. (2018). Constraining the evolution of Neogene ocean carbonate chemistry using the boron isotope pH proxy. *Earth and Planetary Science Letters, 498*, 362-376. https://doi.org/10.1016/j.epsl.2018.06.017

Vogl, J., & Rosner, M. (2012). Production and certification of a unique set of isotope and delta reference materials for boron isotope determination in geochemical, environmental and industrial materials. *Geostandards & Geoanalytical Research, 36*, 161-175. https://doi.org/10.1111/j.1751-908X.2011.00136.x

Yao, T. D., Masson-Delmotte, V., Gao, J., Yu, W. S., Yang, X. X., Risi, C., et al. (2013). A review of climatic controls on $\delta^{18}O$ in precipitation over the Tibetan Plateau: Observations and simulations. *Reviews of Geophysics, 51*, 525-548. https://doi:10.1002/rog.20023

Zhang, J. W., Yan, Y. N., Zhao, Z. Q., Li, X. D., Guo, J. Y., Ding, H., et al. (2021). Spatial and seasonal variations of dissolved arsenic in the Yarlung Tsangpo River, southern Tibetan Plateau. *Science of The Total Environment, 760*, 143416. https://doi.org/10.1016/j.scitotenv.2020.143416

Zhang, J. W., Yan, Y.N., Zhao, Z.Q., Liu, X. M., Li, X. D., Zhang, D., et al. (2022). Spatiotemporal variation of Li isotopes in the Yarlung Tsangpo Riverbasin (upper reaches of the Brahmaputra River): Source and process. *Earth and Planetary Science Letters,* 600, 117875. https://doi.org/10.1016/j.epsl.2022.117875

Zhang, W. J., Tan, H. B., Zhang, Y. F., Wei, H. Z., & Dong, T. (2015). Boron geochemistry from some typical Tibetan hydrothermal systems: Origin and isotopic fractionation. *Applied Geochemistry, 63*, 436-445. https://doi.org/10.1016/j.apgeochem.2015.10.006

Figure captions

Fig. 1. Geological map and sampling locations along the Yarlung Tsangpo-Brahmaputra River. Green stars are sites of geothermal water samples, and red solid and white circles are sites of river water samples from the mainstream and tributaries, respectively.

Fig. 2. Maps of (a) elevation, (b) precipitation, and (c) air temperature within the Yarlung Tsangpo Basin. The size of green stars and circles in Fig. 2a, 2b, and 2c stands for the elevation, B concentrations, and $\delta^{11}B$ of geothermal samples and river water samples, respectively.

Fig. 3. Crossplot between the reciprocal of dissolved [B] and $\delta^{11}B$ of global geothermal waters compared with those of global rivers. [B] is B concentration expressed in μmol/L. Geothermal water data are from Palmer and Sturchio, 1990; Kasemann, 2004; Millot et al., 2012; Louva et al., 2014; Lü et al., 2014; Zhang et al., 2015; Sosdian et al., 2018. Data for global rivers are from Rose et al. 2000; Lemarchand et al. 2002; Chetelat and Gaillardet, 2005; Lemarchand and Gaillardet, 2006; Chetelat et al., 2009; Liu et al., 2012; Louvat et al., 2011, 2014; Ercolani et al., 2019.

Fig. 4. Seasonal differences in the geochemical signature of water in the Yarlung Tsangpo River. a, B/Cl *vs.* 1000*As/Cl molar ratio. b, B/Cl molar ratio *vs.* $\delta^{11}B$. c, B concentration *vs*. water discharge. d, $\delta^{11}B$ versus water discharge. Error bars for $\delta^{11}B$ in Fig. 4b and 4d represent the 2 s.d. analytical uncertainty.

Fig. 5. Sensitivity tests for the influence of geothermal B input on oceanic $\delta^{11}B_{sw}$. (a) Estimation of the changes of geothermal input required to explain the observed 3‰ change of Cenozoic $\delta^{11}B_{sw}$ ($\Delta\delta^{11}B_{sw}$). (b) Secular $\delta^{11}B_{sw}$ changes during the Cenozoic (Lemarchand et al., 2002) compared with collision-related magmatism in the Tibet reflected as proxied by the degree of melting of local igneous rocks over the last 50 Ma (Guo et al., 2021). The green, blue and orange curves with arrows in Fig. 5a represent the results using lower bound, upper bound and average estimates for the relative contribution of geothermal waters in the global riverine ocean budget, respectively. The numbers at both ends of the curves represent the B input fluxes in Tg B/yr.

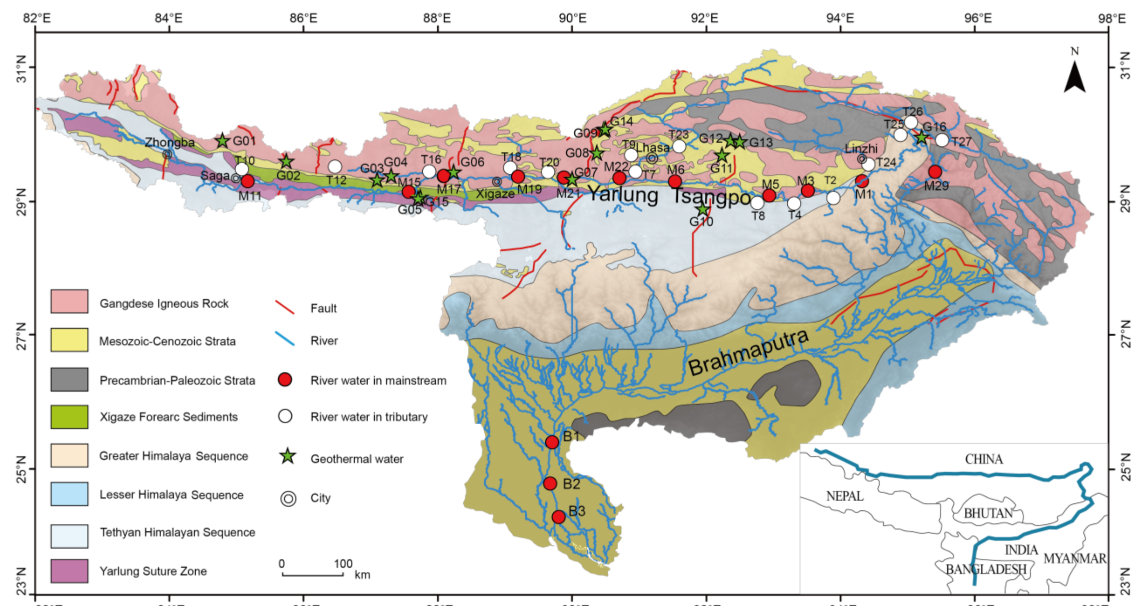

Fig. 1. Geological map and sampling locations along the Yarlung Tsangpo-Brahmaputra River. Green stars are sites of geothermal water samples, and red solid and white circles are sites of river water samples from the mainstream and tributaries, respectively.

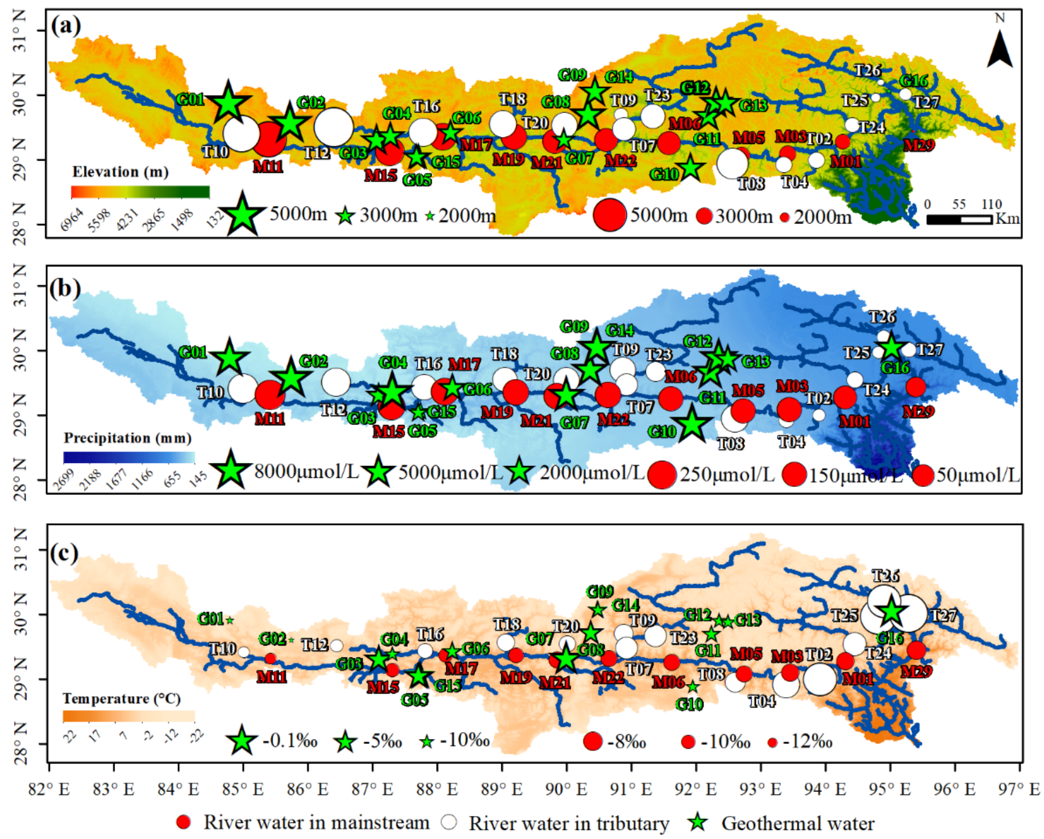

Fig. 2. Maps of (a) elevation, (b) precipitation, and (c) air temperature within the Yarlung Tsangpo Basin.The size of green stars and circles in Fig. 2a, 2b, and 2c stands for the elevation, B concentrations, and $\delta^{11}B$ of geothermal samples and river water samples, respectively.

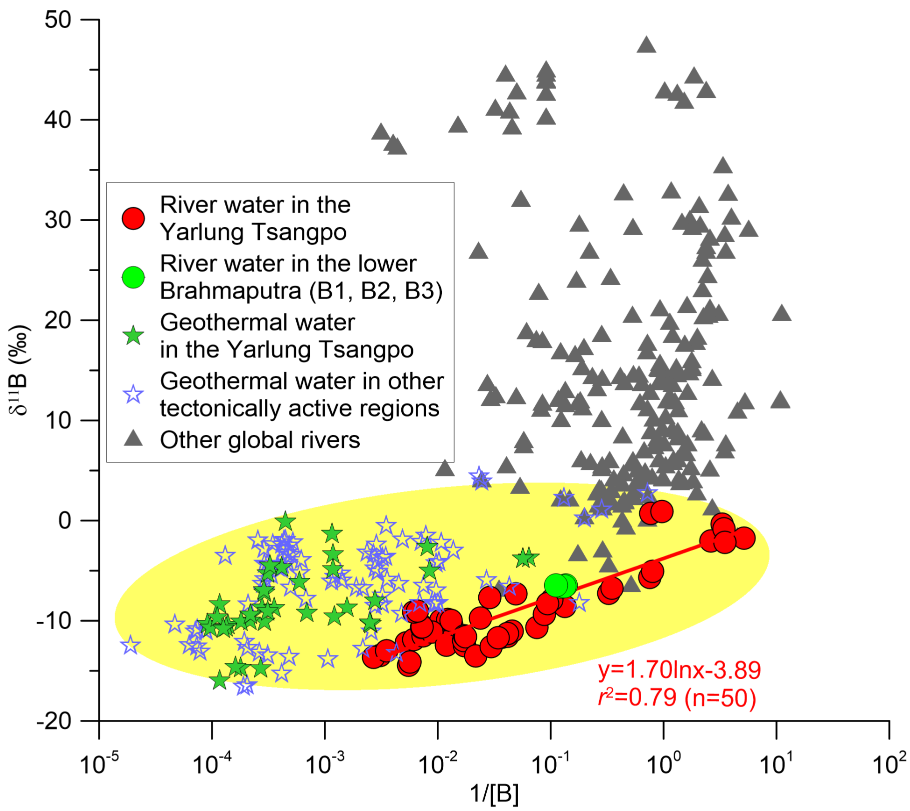

Fig. 3. Crossplot between the reciprocal of dissolved [B] and δ^{11}B of global geothermal waters compared with those of global rivers. [B] is B concentration expressed in μmol/L. Geothermal water data are from Palmer and Sturchio, 1990; Kasemann, 2004; Millot et al., 2012; Louva et al., 2014; Lü et al., 2014; Zhang et al., 2015; Sosdian et al., 2018. Data for global rivers are from Rose et al. 2000; Lemarchand et al. 2002; Chetelat and Gaillardet, 2005; Lemarchand and Gaillardet, 2006; Chetelat et al., 2009; Liu et al., 2012; Louvat et al., 2011, 2014; Ercolani et al., 2019.

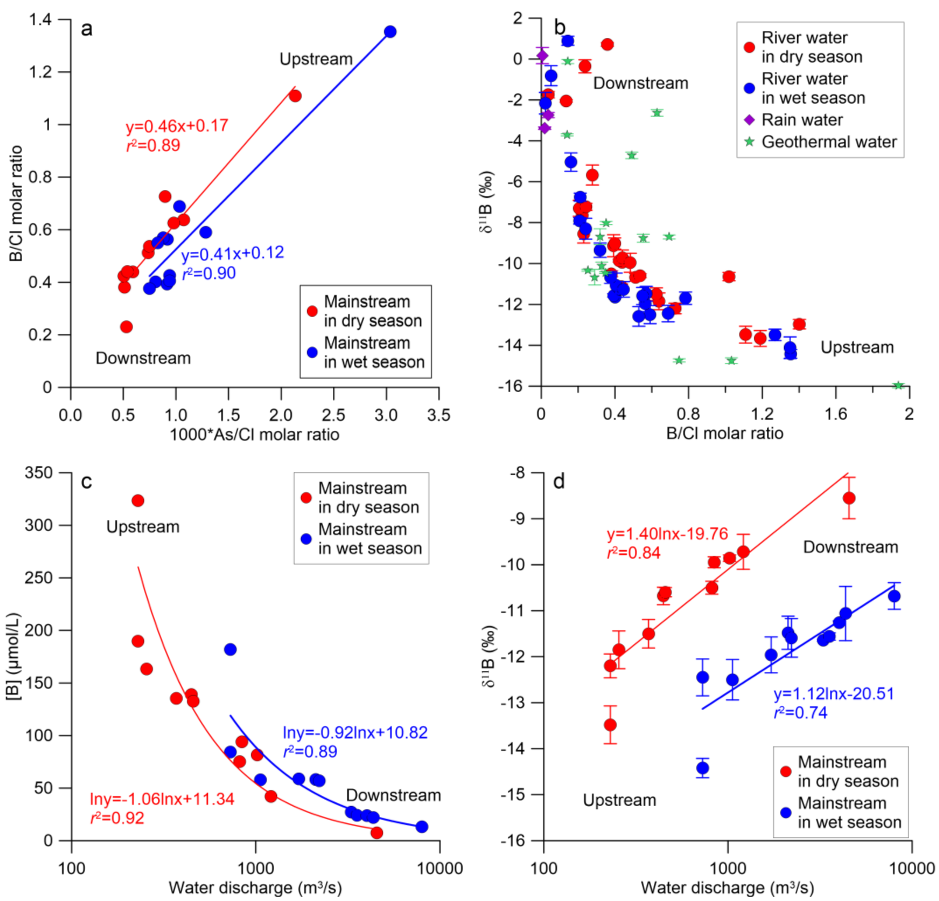

Fig. 4. Seasonal differences in the geochemical signature of water in the Yarlung Tsangpo River. a, B/Cl *vs.* 1000*As/Cl molar ratio. b, B/Cl molar ratio *vs.* δ^{11}B. c, B concentration *vs.* water discharge. d, δ^{11}B versus water discharge. Error bars for δ^{11}B in Fig. 4b and 4d represent the 2 s.d. analytical uncertainty.

35

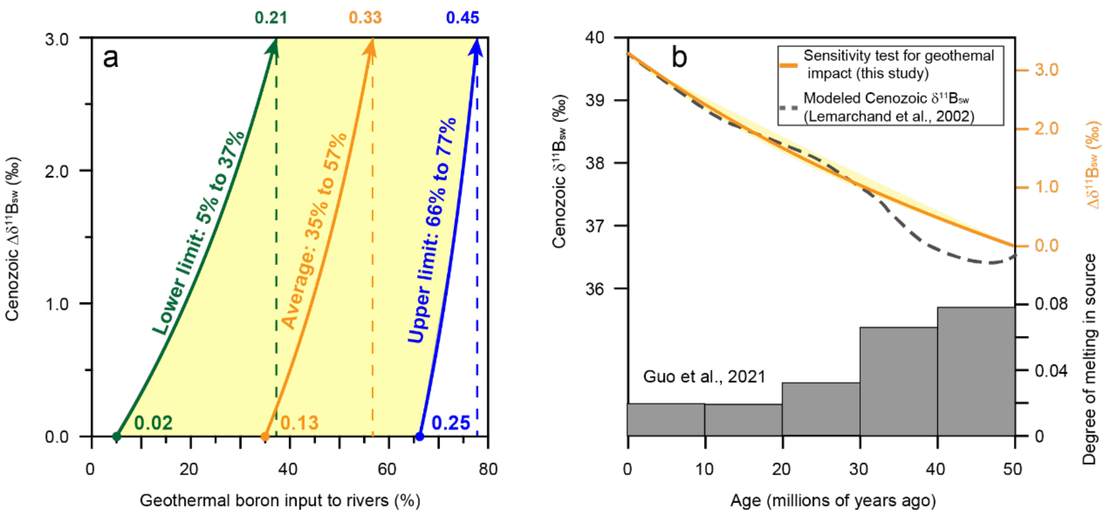

Fig. 5. Sensitivity tests for influence of geothermal B input on oceanic $\delta^{11}B_{sw}$. (a) Estimation on the changes of geothermal input required to explain the observed 3‰ change of Cenozoic $\delta^{11}B_{sw}$ ($\Delta\delta^{11}B_{sw}$). (b) Secular $\delta^{11}B_{sw}$ changes during the Cenozoic (Lemarchand et al., 2002) compared with collision-related magmatism in the Tibet reflected as proxied by the degree of melting of local igneous rocks over the last 50 Ma (Guo et al., 2021). The green, blue and orange curves with arrows in Fig. 5a represent the results using lower bound, upper bound and average estimates for the relative contribution of geothermal waters in the global riverine ocean budget, respectively. The numbers at both ends of the curves represent the B input fluxes in Tg B/yr.